Convectons

Arantxa Alonso, Oriol Batiste, Edgar Knobloch and Isabel Mercader

Abstract A horizontal layer containing a miscible mixture of two fluids can generate dissipative solitons called convectons when heated from below. The physics of the system leading to this behavior is explained, and the properties of the resulting convectons are described. The convectons are shown to be present in a parameter regime known as the pinning region containing a multiplicity of stable convectons of odd and even parity. These lie on solution branches that snake back and forth across the pinning region and illustrate a phenomenon known as homoclinic snaking. Examples of single pulse and multipulse convectons in periodic and closed containers are exhibited and compared with similar states described by the Swift-Hohenberg equation. Time-dependent states in the form of localized traveling waves are computed and distinguished from convectons that drift.

1 Introduction

Many fluid systems exhibit spatially localized structures in both two [29]–[3] and three [15, 40] dimensions. Of these the localized structures or *convectons* arising in binary fluid convection are perhaps the best studied. These states are similar to localized structures studied in other areas of physics [2] despite the fact that fluid systems must always be confined between boundaries. On the other hand in fluid systems the length scale is typically set by the layer depth or the distance between any confining boundaries instead of being an intrinsic length scale selected by a Turing or modulational instability. As a result when we speak of localized states in binary fluid convection we mean states that are localized in the horizontal direction only. In this

Arantxa Alonso, Oriol Batiste, Isabel Mercader
Departament de Física Aplicada, Universitat Politècnica de Catalunya, Barcelona, Spain

Edgar Knobloch
Department of Physics, University of California, Berkeley CA 94720, USA

sense the problem resembles laser systems in short cavities in which the standing wave structure in the longitudinal direction remains of paramount importance [28].

In fluids dissipation, whether through viscosity or thermal diffusion, is generally of great importance. For example, it is responsible for the presence of a nonzero threshold value of the Rayleigh number, a dimensionless measure of thermal forcing, for convection to occur. As a result the dissipative solitons of interest in the present article are strongly dissipative and hence require strong forcing for their maintenance. States of this type cannot be understood in terms of (an infinite-dimensional) Hamiltonian system with small forcing and dissipation.

In this article we survey the properties of localized states in binary fluid convection in a horizontal layer of depth h heated from below. Binary liquids, such as water-ethanol [36, 49] and water-salt mixtures [22] or mixtures of He^3-He^4 at cryogenic temperatures [1], are characterized by a cross-diffusion effect called the Soret effect that describes the diffusive separation of the lighter and heavier molecular weight components of the mixture in an imposed temperature gradient. Specifically, if C is the concentration of the heavier component then its flux is proportional to $-\nabla C - C_0(1-C_0)S_T\nabla T$, where S_T is the Soret coefficient, T is the temperature and C_0, $0 < C_0 < 1$, is the mean concentration. Thus when $S_T > 0$ the heavier component migrates, on a diffusive time scale, towards the colder boundary and vice versa. On the other hand, in the anomalous case in which $S_T < 0$ the heavier component migrates towards the hotter boundary. As a result if a mixture with a negative Soret coefficient is heated from below the destabilizing temperature gradient sets up, in response, a stabilizing concentration distribution. The competition between these two effects leads to complex behavior, including time-dependence at onset of convection [34, 8].

In the absence of motion the temperature T satisfies Laplace's equation. When the top and bottom plates confining the fluid have a larger heat capacity than the fluid the boundaries may be considered to be good thermal conductors in the sense that any fluid motion will not significantly distort the temperature of the plates. Under these circumstances we may suppose, to a good approximation, that the temperature of the bounding plates is fixed, $T = T_0 + (\Delta T/2)$ at $z = 0$ and $T = T_0 - (\Delta T/2)$ at $z = h$. In the conduction state the temperature distribution is therefore $T(z) = T_0 + \Delta T[(1/2) - (z/h)]$. Convection distorts this conduction profile and we write $T(x,z,t) = T_0 + \Delta T[(1/2) - (z/h) + \theta(x,z,t)]$, where $\theta(x,z,t)$ captures the effects of the fluid motion. Owing to the Soret effect the conduction state is also associated with a concentration distribution of the heavier molecular weight component, $C(z) = C_0 + \Delta C[(1/2) - (z/h)]$, where $\Delta C = -C_0(1-C_0)S_T\Delta T$, and we write $C(x,z,t) = C_0 + \Delta C[(1/2) - (z/h) + \Sigma(x,z,t)]$ to describe the stirring effect of the fluid motion. It is tempting to think of ΔC as an imposed concentration difference across the layer, but this is incorrect since the boundary conditions on C are not that C is fixed on the boundaries but that the flux of the heavier component vanishes on the boundaries, i.e., that $\eta_z = 0$ on $z = 0, 1$, where $\eta \equiv \theta - \Sigma$.

In the following we nondimensionalize the governing equations using the depth h as the unit of length and the thermal diffusion time h^2/κ in the vertical as the unit of time. The system is then described by the dimensionless equations [9]

$$\mathbf{u}_t + (\mathbf{u}\cdot\nabla)\mathbf{u} = -\nabla P + \sigma R[(1+S)\theta - S\eta]\hat{\mathbf{z}} + \sigma\nabla^2\mathbf{u}, \quad (1)$$

$$\theta_t + (\mathbf{u}\cdot\nabla)\theta = w + \nabla^2\theta, \quad (2)$$

$$\eta_t + (\mathbf{u}\cdot\nabla)\eta = \tau\nabla^2\eta + \nabla^2\theta, \quad (3)$$

together with the incompressibility condition $\nabla\cdot\mathbf{u} = 0$. Here $\mathbf{u} \equiv (u,w)$ is the dimensionless velocity field in (x,z) coordinates and P is the pressure. The system is specified by four dimensionless parameters,

$$R \equiv \frac{\alpha g \Delta T h^3}{\kappa\nu}, \quad S \equiv \frac{\beta}{\alpha} C_0(1-C_0)S_T, \quad \sigma \equiv \frac{\nu}{\kappa}, \quad \tau \equiv \frac{D}{\kappa}, \quad (4)$$

referred to, respectively, as the Rayleigh number, separation ratio, Prandtl number and Lewis number. Here $\alpha \equiv -\rho_0^{-1}(\partial\rho/\partial T)_0 > 0$ is the coefficient of thermal expansion, $\beta \equiv \rho_0^{-1}(\partial\rho/\partial C)_0 > 0$ is the corresponding coefficient describing the concentration dependence of the fluid density ρ, g is the acceleration due to gravity, ν is the kinematic viscosity and D is the molecular diffusivity of the heavier component; the subscript 0 indicates reference values, computed at $T = T_0$, $C = C_0$. Thus σ and τ specify the properties of the fluid (typically for liquids $\sigma = O(1)$ while $\tau = O(10^{-2})$), while the parameter R specifies the strength of the applied temperature difference imposed across the system, and plays the role of an easily controllable bifurcation parameter. The parameter S is proportional to the Soret coefficient S_T and characterizes the mixture since it measures the concentration contribution to the buoyancy force due to cross-diffusion.

When S or equivalently S_T is sufficiently negative, (i) the primary steady state bifurcation becomes subcritical since any convection that mixes the two components will decrease the stabilizing effect of the concentration stratification produced in response to the destabilizing thermal stratification, and hence make convection easier, and (ii) the primary instability of the conduction state $\mathbf{u} = \theta = \eta = 0$ becomes a Hopf bifurcation [33]. With periodic boundary conditions and identical boundary conditions at the top and bottom this bifurcation is a Hopf bifurcation with $\mathrm{O}(2)\times Z_2$ symmetry, where $R_x \in \mathrm{O}(2)$ acts by $(u(x,z),\, w(x,z),\, \theta(x,z),\, \eta(x,z)) \to (-u(-x,z),\, w(-x,z),\, \theta(-x,z),\, \eta(-x,z))$ relative to a suitable origin, and $R_z \in Z_2$ acts by $(u(x,z),\, w(x,z),\, \theta(x,z),\, \eta(x,z)) \to (u(x,1-z),\, -w(x,1-z),\, -\theta(x,1-z),\, -\eta(x,1-z))$; the continuous part of the symmetry O(2) corresponds to translations in x. The presence of this symmetry is important, and is responsible, for example, for the bifurcation of a circle of periodic states from the conduction state at the primary bifurcation. Its effect on the Hopf bifurcation is more profound [31]: the bifurcation results in two branches of time-dependent oscillations, traveling waves (hereafter, TW) and standing waves (hereafter, SW) both of which typically bifurcate subcritically and are unstable [24], although the TW may acquire stability at finite amplitude. In contrast, in a closed container this bifurcation breaks apart into successive bifurcations to time-periodic *chevron* states called $\mathrm{SW}_{0,\pi}$. These states are characterized by the presence of a source in the center of the container that emits waves that travel outwards towards the boundaries; the waves may be emitted either in phase (SW_0) or out of phase (SW_π) [26, 7]. The appearance of chevrons

already within linear theory is a consequence of a boundary-induced change in the unstable eigenfunction [7]. Moreover, the imposition of lateral boundaries shifts the bifurcation to TW-like states to finite amplitude: these states are no longer *rotating waves* but they break the symmetry of the chevron states, i.e., these are states in which one or other propagation direction predominates. In addition, entirely new states may arise through a secondary Hopf bifurcation from one of the chevron states. These states, called *blinking* states [8, 6], consist of waves that periodically reverse direction, and have no analogue in the corresponding problem on a periodic domain. Indeed, the presence of these states can be related to the loss of translation invariance when lateral boundaries are imposed. A detailed discussion of the effect of such boundaries on the Hopf bifurcation can be found in [26].

In periodic domains with larger spatial period the TW typically lose coherence and break up into a spatio-temporally chaotic state known as dispersive chaos [6]–[39].

In the following we describe some solutions of Eqs. (1)-(3) with the boundary conditions $\mathbf{u} = \theta = \eta_z = 0$ on $z = 0, 1$ appropriate to no-slip, fixed temperature, no-mass-flux boundary conditions, and either (i) periodic boundary conditions (hereafter, PBC) in the horizontal with dimensionless period Γ, (ii) Neumann or stress-free boundary conditions (hereafter, NBC) $u = w_x = \theta_x = \eta_x = 0$ on $x = \pm\Gamma/2$, or (iii) insulating closed container boundary conditions (hereafter, ICCBC), $\mathbf{u} = \theta_x = \eta_x = 0$ on $x = \pm\Gamma/2$. Only a single horizontal dimension will be included resulting in patterns that are two-dimensional, with one extended dimension only. The results described below are for parameter values that have been used in experiments on water-ethanol mixtures.

2 Convectons with periodic boundary conditions

In Fig. 1(a) we show the results for a $\Gamma = 60$ periodic domain with the parameters $S = -0.021$, $\sigma = 6.22$, $\tau = 0.009$ used in [37]. The figure represents a bifurcation diagram that shows the dimensionless convective heat flux across the layer as a function of the imposed Rayleigh number R. Steady spatially periodic overturning convection (hereafter, SOC) is strongly subcritical, and acquires stability (solid line) above the termination point of the TW branch. The latter bifurcates subcritically from the primary Hopf bifurcation at $R = R_H \approx 1760.8$ corresponding to the onset of convective instability; the SW are not shown. Dispersive chaos is present for $R > R_H$ and is stable; this state is indicated in Fig. 1(a) using solid dots. The time-independent convectons discussed below emerge from this state with increasing R via relaxation oscillations as described in [9]. Figure 1(b) shows a typical transient once stable convectons are present, showing the decay of dispersive chaos into a stable, time-independent convecton. The growth of this structure suppresses motion outside the convecton. Thus the formation of the convecton may be viewed as a type of nonlinear focusing instability. The void region outside the convecton fills with waves if the convecton region extends beyond the absolute instability threshold [9].

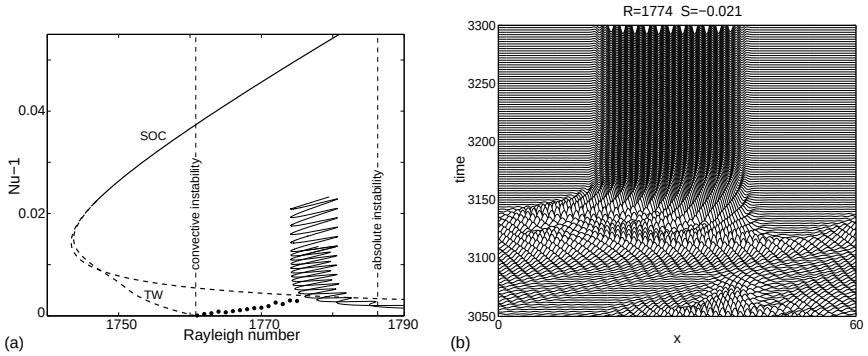

Fig. 1 (a) Bifurcation diagram showing the time-averaged convective heat flux per unit length across the layer, $Nu-1 \equiv \Gamma^{-1}\int_{-\Gamma/2}^{\Gamma/2} \theta_z(x,z=1)\,dx$, as a function of the Rayleigh number R when $\Gamma = 60$. The conduction state loses instability at a Hopf bifurcation ($R = R_H \approx 1760.8$). Steady spatially periodic convection (SOC) acquires stability at a parity breaking bifurcation marking the destruction of a branch of spatially periodic traveling waves (TW) originating in the primary bifurcation. Small amplitude dispersive chaos (solid dots) is present for $R > R_H$ and leads into the pinning region ($1774 < R < 1781$) containing a multiplicity of stable localized states of both even and odd parity. (b) Space-time plot showing the midplane temperature $\theta(x,z=1/2,t)$ as a function of time for $R = 1774$ starting from a random small amplitude initial condition. Parameters: $S = -0.021$, $\sigma = 6.22$, $\tau = 0.009$, $\Gamma = 60$. From Ref. [9].

Figure 1(a) reveals that the convectons are organized into a pair of branches corresponding to steady states with well defined parity: even states are invariant under R_x and satisfy $(u(x,z),\, w(x,z),\, \theta(x,z),\, \eta(x,z)) = (-u(-x,z),\, w(-x,z),\, \theta(-x,z),\, \eta(-x,z))$, while odd states are invariant under $R_x \circ R_z$ and satisfy $(u(x,z),\, w(x,z),\, \theta(x,z),\, \eta(x,z)) = -(u(-x,1-z),\, w(-x,1-z),\, \theta(-x,1-z),\, \eta(-x,1-z))$. These branches, L_{even} and L_{odd}, respectively, snake back and forth across an interval of Rayleigh numbers called the snaking or pinning region. This interval is quite small for the separation ratio used here, but widens as $|S|$ increases. The pinning region contains a large multiplicity of stable convectons of different lengths and either parity. However, the pinning regions for the even and odd parity convectons are not identical – the pinning region for the odd convectons is generally noticeably narrower than that of even parity convectons [9, 41, 42].

To understand the properties of these states we show in Fig. 2 a series of convectons computed in a smaller domain, with period $\Gamma = 14$. The states are visualized in terms of contours of constant temperature fluctuation θ and contours of constant concentration C. Here and elsewhere all solution profiles use the same color table to indicate the amplitude of the temperature and concentration fields. The figure shows even and odd convectons at successive saddle-nodes on the L_{even} and L_{odd} branches (not shown). The figure reveals that the end vortices repeatedly change direction as one proceeds upwards, from saddle-node to saddle-node, along the right boundary of the pinning region, as additional vortices are nucleated pairwise at the edges of each convecton. As a result the convectons at the right boundary are characterized

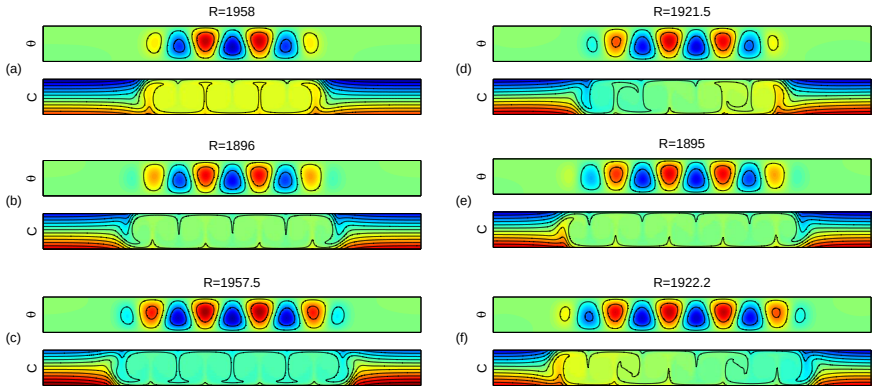

Fig. 2 (Color online) (a)-(c) Even parity convectons at successive saddle-nodes on the L_{even} branch with PBC. States (a,c) are on the right of the pinning region, while (b) is on the left. (d)-(f) Odd parity convectons at successive saddle-nodes on the L_{odd} branch with PBC. States (d,f) are on the right of the pinning region, while (e) is on the left. The states are visualized in terms of contours of constant temperature fluctuation θ and contours of constant concentration C. Here and elsewhere all solution profiles use the same color table to indicate the amplitude of the temperature and concentration fields. The states on the right of the pinning region are characterized by strong vortices at either end of the structure and hence strong entrainment; those on the left of the pinning region have weak vortices in the front regions, and very little concentration is entrained. Parameters: $S = -0.1$, $\sigma = 7$, $\tau = 0.01$, $\Gamma = 14$. From Ref. [42].

by strong entrainment of concentration, leading either to a change in the mean concentration within the convecton (even parity convectons) or a concentration gradient within the convecton (odd parity convectons). In contrast, the saddle-nodes along the left boundary correspond to transitions between successive states, and at these the end vortices are very weak, with almost no entrainment taking place (Fig. 2). Thus the convectons on the left of the pinning region are characterized by homogenized concentration that is equal to the average concentration.

Figure 3 indicates that the convectons form by excavating a hole in the concentration distribution much as described for localized traveling waves by Riecke [46]. This self-trapping resembles closely what happens in optical systems when a laser "burns" a hole through a nonlinear medium by locally altering the index of refraction. In general these types of mechanisms are associated with a finite threshold – in our language they are subcritical. This is the case for the SOC branch in the binary convection problem since an increase in the convection amplitude increases the mixing of the concentration field thereby decreasing its stabilizing effect and allowing convection to proceed at lower Rayleigh numbers. Moreover, when convection is enhanced locally the same process may result in the formation of a localized structure, at least within a well-defined range of Rayleigh numbers. Figure 3 also shows that the convecton profile, once formed, is insensitive to the spatial period Γ. This period only serves to define the available supply of C that can be pumped horizontally by odd convectons or entrained by even convectons.

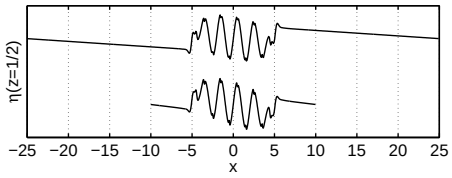

Fig. 3 Profiles of $\eta(x, z = 1/2)$ for odd parity convectons of the same length at $R = 1919$ in domains with PBC and $\Gamma = 20, 50$. The profiles are identical except for an overall offset due to different values of the horizontal midplane concentration jump across the convectons generated by the flow within. Parameters: $S = -0.1$, $\sigma = 7$, $\tau = 0.01$.

3 Convectons with ICCBC

When the boundary conditions are changed to ICCBC (or CCBC as in [41]) the translation invariance is broken and the symmetry that remains is the symmetry $Z_2 \times Z_2 \sim D_2$ generated by R_x and R_z. Figures 4(a,b) show the bifurcation diagrams for (a) even and (b) odd states in a $\Gamma = 14$ domain when ICCBC are imposed at $x = \pm\Gamma/2$ and compare the results with those of the corresponding PBC case. As discussed in [41, 42] the traditional snaking diagram is greatly perturbed by this type of boundary condition. Instead of coexistence between snaking and periodic branches the snaking branches now turn continuously into large amplitude states that take the place of the competing periodic states. These large amplitude states fill the container but are not periodic – instead they contain defects that allow the state to adjust to the imposed boundary conditions – and in this they resemble states known as mixed mode states that are also present in the PBC case [42, 13]. This is so for both even (Fig. 4a) and odd (Fig. 4b) parity states. Localized states computed with ICCBC at successive saddle-nodes are shown in Fig. 5. In addition, the ICCBC

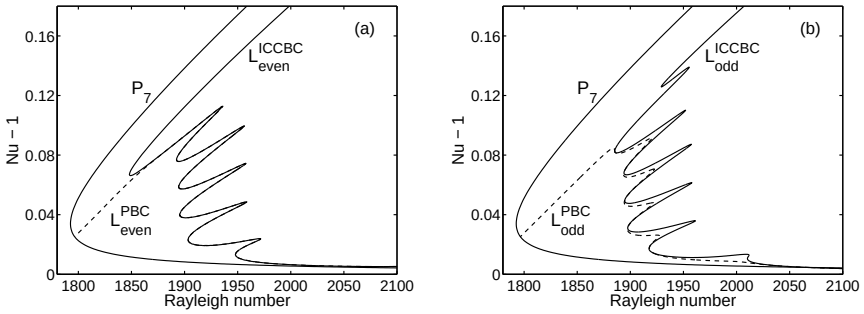

Fig. 4 Comparison of the bifurcation diagrams in a $\Gamma = 14$ domain with PBC and ICCBC. (a) Even parity localized states; the two branches coincide until the domain is almost filled. (b) Odd parity localized states; the two branches differ throughout as a consequence of the suppression of horizontal pumping by odd convectons in the presence of ICCBC. Parameters: $S = -0.1$, $\sigma = 7$, $\tau = 0.01$. From Ref. [42].

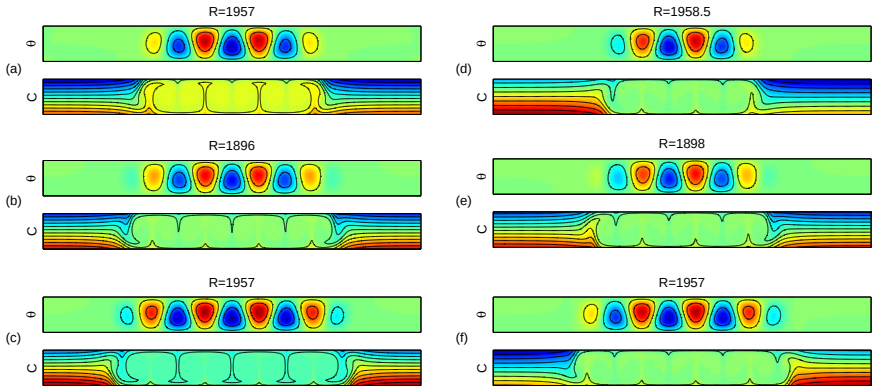

Fig. 5 (Color online) (a)-(c) Even parity convectons with ICCBC in a $\Gamma = 14$ container at successive saddle-nodes on the L_{even} branch. States (a,c) are on the right of the pinning region, while (b) is on the left. (d)-(f) Odd parity convectons with ICCBC in a $\Gamma = 14$ container at successive saddle-nodes on the L_{odd} branch. States (d,f) are on the right of the pinning region, while (e) is on the left. The states on the right of the pinning region are characterized by strong vortices at either end of the structure and hence strong entrainment; those on the left of the pinning region have weak vortices in the front regions, and very little concentration is entrained. Parameters: $S = -0.1$, $\sigma = 7$, $\tau = 0.01$. From Ref. [42].

increase substantially the width of the pinning region for the odd parity states and hence exert an effect on odd parity convectons even when the convectons are localized well away from the walls. Indeed, the width of the pinning region for the odd parity states is now identical to that of even parity states [41, 42].

Figure 4(a) shows that until the domain fills with convection the even parity convecton branches with ICCBC and PBC track one another very closely, indicating that the pinning of the fronts to the structured state between them that is responsible for the snaking behavior of the convecton branches is unaffected by the lateral walls whenever the convecton has even parity. Figure 4(b) shows that this is not the case for odd parity convectons, suggesting that the horizontal pumping of concentration by odd parity convectons is responsible [41]. However, the snaking behavior with ICCBC still resembles the PBC case qualitatively, and indeed the left boundaries of the two pinning regions coincide (see below).

As explained in [41] odd parity convectons in the presence of closed container boundary conditions should be thought of as being one half of a two-convecton state filling a domain of length 2Γ obtained by reflecting the odd convecton in $x = \pm\Gamma/2$. Such a reflection yields exact solutions in the case of Neumann boundary conditions and results in a state in which the pumping effects of oppositely oriented odd convectons cancel out, producing a more or less spatially uniform concentration (and temperature) in the void region between them (Figs. 5d,f), and eliminating the mean concentration gradient present in odd convectons computed with PBC (Figs. 2d,f). The concentration level on either side of the convecton depends on whether the convectons pump towards one another or away from one another, and

in a domain of period 2Γ the resulting concentration jump balances the pumping action of the individual convectons. It is for this reason that the two-convecton state with equidistant convectons matches, at least approximately, the solutions found here with insulating no-slip boundary conditions at $x = \pm\Gamma/2$.

To confirm this scenario we examined in [42] the flux balance in the fore and aft regions of the odd parity convecton shown in Fig. 5(d). We denote the midplane concentration to the left of the convecton by C^- and to the right by C^+; the mean midplane concentration inside the convecton is $\bar{C}$. We suppose that the convecton pumps concentration from right to left with flux F. Then flux balance at the left front of the convecton, required for the existence of a steady state, leads to the estimate $F \approx \tau(C^- - \bar{C})/\delta$, while that at the right front leads to $F \approx \tau(\bar{C} - C^+)/\delta$. Here δ is the width of the front region, assumed to be the same fore and aft. It follows that $\bar{C} \approx (C^+ + C^-)/2$, a conclusion that agrees very well with the computations shown in Figs. 5(d,f). The same argument applied to odd or even convectons at a left saddle-node leads to the prediction $C^- = \bar{C} = C^+$ since $F = 0$ (no entrainment by end vortices). This is so for both PBC (Fig. 2) and ICCBC (Fig. 5) since the boundary conditions exert little influence when $F = 0$, in agreement with the computations reported in Figs. 2(b,e) and Figs. 5(b,e). This prediction explains, moreover, why the left boundary of the pinning region for odd convectons is unaffected by the boundary conditions (Fig. 4b) – and hence coincides with the left boundary of the even convecton snaking region – while the right boundary is affected dramatically. Finally, the above argument also explains the depletion of the concentration outside the even convecton in Fig. 5(a) and its enhancement outside the even convecton in Fig. 5(c).

In Fig. 6(a) we show a different type of convecton. This convecton is also computed with ICCBC but instead of being located in the center of the container it is

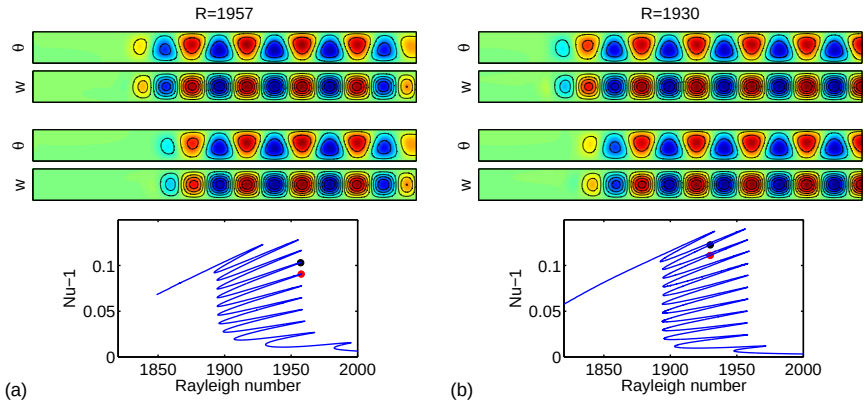

Fig. 6 Wall-attached convectons with (a) ICCBC, and (b) NBC in terms of $\theta(x,z)$ and $w(x,z)$. The corresponding bifurcation diagrams are shown at the bottom, with the black dots referring to the (longer) upper states and the red dots referring to the (shorter) states in the middle panels. Parameters: $S = -0.1$, $\sigma = 7$, $\tau = 0.01$. From Ref. [43].

attached to one of the walls. Despite this difference the branch of these convectons also snakes, and with each turn a new cell appears at the free end of the convecton. As a result the direction of the entraining vortex changes at each turn, and so does the homogenized concentration within the structure (Fig. 6a). In contrast, the center convectons such as those shown in Fig. 5(a) grow by adding a *pair* of cells, one on each side, and so undergo only half the number of back and forth oscillations before the domain is filled as the wall-attached convectons.

To understand the origin of the wall-attached convecton we show in Fig. 6(b) the corresponding state with NBC. These (unphysical) boundary conditions allow one to reflect the structure in the boundary $x = \Gamma/2$ and obtain a continuous solution of Eqs. (1)-(3) on the doubled domain, i.e., an even convecton located in the center of a domain of period 2Γ. Structures of this type are well understood, and in particular snake in the usual fashion. Since the domain is twice as large the convecton branch with NBC undergoes twice as many back and forth oscillations before the domain is filled as an even convecton branch in a domain of length Γ, and this fact is reflected in the number of turns executed by the solution branch in Fig. 6(b). This behavior in turn resembles closely that observed in Fig. 6(a) even though the latter states cannot be reflected in the boundary $x = \Gamma/2$. It should be mentioned that the temperature field $\theta(x,z)$ does not fully reveal the difference between ICCBC and NBC solutions which is more visible in the velocity field $w(x,z)$ since $w(\pm\Gamma/2,z) = 0$ in the former but not in the latter (Figs. 6a,b).

4 Multiconvectons

In Fig. 7 we show bound states of two convectons in a domain with NBC at $x = 0,\Gamma$. Figure 7(a) shows a state consisting of two "even" parity convectons of opposite sign, where the sign refers to the direction of the outer cells. In fact the individual convectons are slightly distorted by their interaction and near the end of the branch (open dot) cease to look even. However, the overall structure has exact odd parity with respect to $x = 0$ and, as expected, also snakes although the snake is not well developed: since the effective domain per convecton is now only $\Gamma/2$ the domain fills up rapidly and the snaking branch terminates on a branch consisting of identical 13 cells with odd parity and a well-defined wavenumber (not shown). Figure 7(b) shows a different odd parity multiconvecton. This one consists of one central odd parity state and two wall-attached convectons related by odd parity. With NBC the structure can be reflected in the end walls and still satisfy Eqs. (1)-(3). The resulting structure consists of an alternating array of odd and even states of opposite sign, and also snakes. This branch also terminates on the odd parity 13 cell branch, at the same location (open dot) as the branch in Figure 7(a) – as the termination point is approached, the voids fill in and the two solutions come to resemble one another. Thus the termination point can be viewed as a bifurcation from a constant amplitude state to different types of hole-like states.

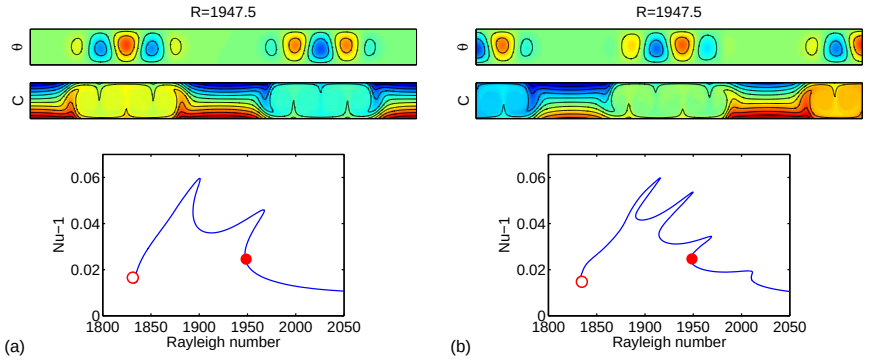

Fig. 7 Odd parity multiconvectons with NBC. (a) A bound pair of "even" parity convectons of opposite sign. (b) A bound pair of "odd" parity convectons. Lower panels show the bifurcation diagrams with the red dot indicating the location of the profile shown in the upper panel. The open dots indicate the termination point of each branch; this point is the same for both branches and lies on a branch with 13 identical cells (not shown). Parameters: $S = -0.1$, $\sigma = 7$, $\tau = 0.01$. From Ref. [43].

5 Localized traveling waves

Figure 8(a) shows the decay of an unstable even parity convecton at $R = 1947$ into a spatially localized traveling wave (hereafter, LTW). Both the waves within the packet and the packet itself travel to the left, although the speed of the latter is quite slow. Wave packets of this type are frequently found in experiments, both in rectangular [44, 30] and periodic [35] domains, and have also been found in simulations [51, 4]. In the present case the LTW coexist with time-independent convectons and the latter evolve into LTW when they are unstable with respect to asymmetric (i.e., phase) perturbations. The LTW are quite different from the drifting localized structures that form when the symmetry of Eqs. (1)-(3) with respect to $x \to -x$ is weakly broken [21]. The latter take the form of solitary waves, i.e., waves that are steady in an appropriately moving reference frame – the speed of this frame must be determined as an eigenvalue of a nonlinear eigenvalue problem. In contrast, the LTW consist of two frequencies, one from the motion of the wave packet and the other from the waves within the packet.

Figure 8(b) shows that in larger domains the LTW can also form bound states; these consist of two or more LTW traveling with a common speed. These states form as a result of the overlap of the oscillatory tails of the leading and trailing structures, and the resulting mutual entrainment. Similar structures form in flowing liquid films [12] and indeed as secondary structures on top of an already developed traveling wave state [48].

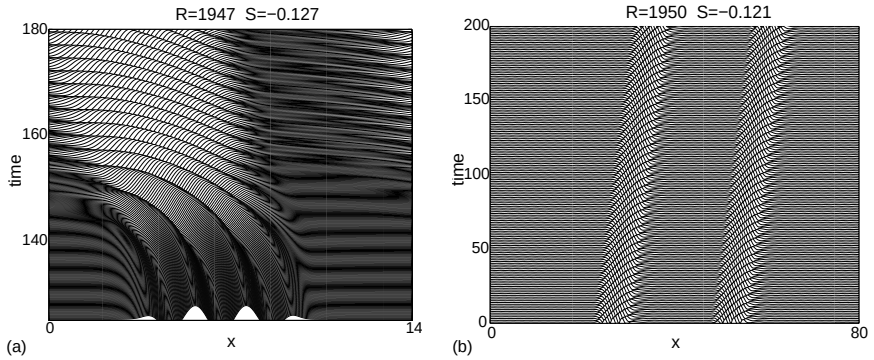

Fig. 8 (a) A space-time plot showing the evolution of an even parity convecton into a spatially localized traveling wave (LTW). (b) A space-time plot showing a bound state of two LTW. Parameters: (a) $R = 1947$, $S = -0.127$, $\Gamma = 14$; (b) $R = 1950$, $S = -0.121$, $\Gamma = 80$.

6 Interpretation

The properties and organization of the states described above resemble those familiar from parallel studies of a much simpler problem, the Swift-Hohenberg equation on the real line,

$$u_t = ru - (\partial_x^2 + 1)^2 u + f(u)\,, \tag{5}$$

where $f(u) = f_{23}(u) \equiv b_2 u^2 - u^3$ (hereafter, SH23) or $f(u) = f_{35}(u) \equiv b_3 u^3 - u^5$ (hereafter, SH35). Like Eqs. (1)-(3) Eq. (5) is reversible with respect to $x \to -x$, $u \to u$; SH35 has, in addition, the symmetry $x \to x$, $u \to -u$ analogous to the midplane symmetry R_z of Eqs. (1)-(3). Both SH23 and SH35 have been extensively studied (see [19] for a review). On the real line, when $b_2 > \sqrt{27/38}$, resp. $b_3 > 0$, the primary branch P of periodic states bifurcates subcritically, and is therefore initially unstable. With increasing amplitude it turns around and acquires stability in a saddle-node bifurcation. At a point M, the Maxwell point, the energy of the state P vanishes and is therefore equal to the energy of the trivial state $u = 0$. At this point, $r = r_M$, fronts can be constructed connecting the $u = 0$ state to P and back again, and consequently steady spatially localized structures of arbitrary length all coexist. However, because the state P is structured, the fronts cannot move freely when r is perturbed from r_M: the fronts are pinned to the heterogeneity of the state P between them [45], and consequently will only move once $|r - r_M|$ becomes sufficiently large. This physical argument relies on the existence of a free energy for SH23 and SH35 but explains why multiple distinct spatially localized equilibria should be present in a "pinning region" surrounding the Maxwell point.

There are in fact two (SH23) or four (SH35) distinct branches of localized states, labeled L_ϕ, and selected by beyond-all-orders effects [38, 23], that bifurcate from $u = 0$ simultaneously with the P branch (Fig. 9). For SH23 $\phi = 0, \pi$, corresponding to even parity states with, respectively, maxima and minima at the symmetry

point $x = 0$. For SH35 there are in addition to $L_{0,\pi}$ also two branches of odd parity states characterized by $\phi = \pi/2$ (positive slope at $x = 0$) and $\phi = 3\pi/2$ (negative slope at $x = 0$). In contrast to SH23 the $\phi = 0, \pi$ solitons are now related by the symmetry $u \to -u$ of SH35 and likewise for the $\phi = \pi/2, 3\pi/2$ solitons. At small amplitude these localized structures are spatially extended but become strongly localized by the time they enter the pinning region. Once in the pinning region the L_ϕ branches begin to snake, adding extra oscillations on either side of each soliton profile while preserving the overall symmetry of the profile. Analysis of the Swift-Hohenberg equation shows that the width of the pinning region is the same for all the snaking branches, and that the wavelength of the periodic structure enclosed within the localized state varies across the pinning region, with the structure compressed for $r < r_M$ and stretched for $r > r_M$ [19]. Stability computations indicate that solitons on branches with a positive slope are stable while those on branches with a negative slope are unstable [17, 18]. The asymmetric states located on the "rungs" connecting the different snaking branches [17, 18] that are responsible for the *snakes-and-ladders* structure of the pinning region are never stable.

Figures 1(a) and 2 show that much of the phenomenology associated with the pinning region as described by SH35 also applies to convection in binary mixtures. This is so despite the fact that the fluid problem is not variational in time, and no energy playing the role of a Lyapunov function can be defined. This is because the snaking behavior shown in Fig. 1(a) is in fact a consequence of the formation of a heteroclinic *cycle* between a trivial state (conduction) and a periodic state (convection), i.e., a solution profile that connects the trivial state at $x = -\infty$ to the periodic state, with a second connection from the periodic state back to the trivial state as $x \to \infty$. In generic systems the formation of this type of orbit is a higher codimension phenomenon but in systems that are *reversible* in space the return connection follows from the equivariance of the equations with respect to $x \to -x$, and the heteroclinic cycle may become generic or *structurally stable*. Numerical computations suggest that this is the case for binary fluid convection: the pinning or snaking interval is filled with heteroclinic connections between the trivial and periodic states. The boundaries of this region correspond to tangencies between the unstable (stable) manifold of the conduction state and the center-stable (center-unstable) manifold of the periodic state [50]–[10]; an energy function is not required at any stage of this argument. Moreover, since the midplane reflection symmetry of Eqs. (1)-(3) with identical boundary conditions at top and bottom plays the same role as the symmetry $u \to -u$ of SH35, four branches of spatially localized convectons bifurcate from the conduction state together with the branch P of periodic states, provided only that the problem is posed on the whole real line. When these are followed numerically by decreasing the Rayleigh number their amplitude grows while their length shrinks. Once their amplitude and length are comparable to the amplitude and wavelength of steady spatially periodic convection on the SOC branch (Fig. 1a) all four convecton branches enter the pinning region and begin to snake back and forth across it (Fig. 1a) as the convectons grow in length by nucleating additional convection rolls at both ends. With periodic boundary conditions in the horizontal this process continues until the length of the convecton becomes comparable to the available

spatial domain when the convecton branches turn over towards the saddle-node of the periodic branch and leave the pinning region [11, 3, 13]. The bifurcation terminating the convecton branches can be interpreted as a bifurcation of holes from a periodic state. Once again there are four branches, with phases $\phi' = 0, \pi/2, \pi, 3\pi/2$. These branches also snake once they enter the pinning region from above and the hole deepens and gradually fills with the conduction state. On the real line these eight snaking branches remain distinct but on periodic domains with finite period they (generally) connect pairwise [13]. Thus in periodic domains of finite period we expect four branches of convectons. For other boundary conditions, it is necessary, however, to distinguish between convectons and holes since these are no longer related by $\Gamma/2$ translation [42, 43].

We mention that we expect rung-like secondary branches to be present in Fig. 1(a) as well. However, in contrast to SH35, in the convection problem these states are expected to correspond to drifting solitary waves, and these are not computed in this article – states of this type are only stationary in SH35 because of its variational structure.

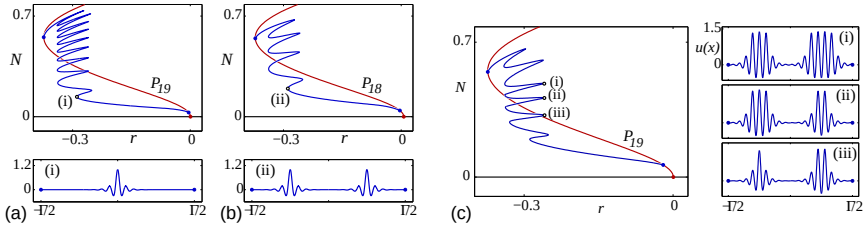

Fig. 9 Bifurcation diagram for the Swift-Hohenberg equation SH23 showing the norm $N \equiv \Gamma^{-1}\int_{-\Gamma/2}^{\Gamma/2} u^2\,dx$ as a function of the parameter r. (a) The branch P_{19} of 19 wavelengths within Γ together with the branch L_0 of convectons with maxima at $x = 0$. (b) Equally spaced two-pulse states cannot bifurcate from P_{19} and instead bifurcate from a subsequent branch P_{18}. Unequally spaced two-pulse states lie on isolas (not shown). (c) Branch of unequal two-pulse states bifurcating from P_{19}. Sample profiles are included. From Ref. [20].

Figure 9(b) shows a branch of two-pulse states computed for SH23 resembling the bound state of two convectons shown in Fig. 7(a) and consisting of two identical equally spaced localized states. For parity reasons this branch cannot bifurcate from the primary branch P_{19} which contains 19 wavelengths per period Γ and so bifurcates from the next branch P_{18} containing 18 wavelengths. Instead the snaking branch that bifurcates from P_{19} corresponds to bound states of nonidentical states as shown in Fig. 9(c) resembling the state shown in Fig. 7(b). However, the correspondence is not precise since SH23 does not have the required additional symmetry $u \to -u$.

The one qualitative difference, beyond the presence of time-dependence, between binary fluid convection and a model equation such as the Swift-Hohenberg equation is the observed difference in the widths of the snaking regions for odd and even par-

ity convectons. This difference increases with increasing $|S|$ since the width of each region increases with the subcriticality of the periodic branch. We have attributed this fact to the pumping effect associated with odd parity convectons whereby heavier fluid is pumped across the convecton from one side to the other depending on the direction of the vortices in the front regions bounding the convectons. In periodic domains this effect necessarily generates a linear concentration profile between adjacent convectons, while in closed containers it leads to convectons with different background concentrations fore and aft. We have seen that the former effect is responsible for the different widths of the snaking regions for odd and even parity convectons and provided a heuristic explanation why this difference disappears in closed containers.

7 Summary

In this article we have summarized the properties of strongly dissipative solitons called convectons that are found in binary fluid convection. We have identified, using a combination of direct numerical simulation and numerical branch following, odd and even convectons in periodic domains, and examined the effects on these structures of lateral boundaries. Because of the horizontal concentration pumping by odd convectons lateral boundaries have a nontrivial effect on the properties of these states and we have explained how and why these boundaries change the width of the pinning region for odd convectons back to that of even convectons. We have also shown examples of wall-attached convectons and different types of two-pulse states. Finally we have shown how these time-independent localized structures relate to localized traveling waves. These results illustrate the richness of this system but in no way represent a systematic study of its properties.

The behavior described here is by no means unique. Stable convectons, including wall-attached convectons, were originally discovered by Ghorayeb and Mojtabi [29] in natural doubly diffusive convection, i.e., convection in a vertical cavity driven by imposed horizontal temperature and concentration differences across the cavity. These states are also associated with snaking behavior [11], this time resembling SH23 since midplane reflection symmetry is now absent [13]. Convection in an imposed vertical magnetic field also exhibits convectons [14, 27] and similar behavior is present in surface tension driven convection in a binary mixture [3]. Similar behavior has been conjectured [32] to be present in other subcritical fluid systems such as plane Couette flow. The reason is simple: the basic mechanism responsible for the creation of these structures is generic in systems that are reversible in space. This is the case for each of the above examples, and provided a heteroclinic cycle between a trivial (homogeneous) and a periodic (structured) state forms as a parameter is varied the associated pinning region in all its richness will be present, and with it the types of behavior described here. Indeed, recent work on plane Couette flow [47] identifies states localized in the cross-stream direction that are of precisely this type. The one significant difference between different fluid systems lies in the stabil-

ity properties of the localized structures. There is in general no reason why stability should follow the predictions from a variational system like the Swift-Hohenberg equation since nonvariational systems admit additional modes of instability. In general this question must be answered on a case by case basis, by explicit stability computations.

Acknowledgements This work was supported by DGICYT under grant FIS2009-08821 and by the National Science Foundation under grant DMS-0908102.

References

1. G. Ahlers and I. Rehberg, Phys. Rev. Lett. **56**, 1373 (1986).
2. N. Akhmediev and A. Ankiewicz (eds), *Dissipative Solitons*, Lect. Notes in Physics **661**, Springer, Berlin (2005).
3. P. Assemat, A. Bergeon and E. Knobloch, Fluid Dyn. Res. **40**, 852 (2008).
4. W. Barten, M. Lücke, M. Kamps and R. Schmitz, Phys. Rev. E **51**, 5662 (1995).
5. O. Batiste and E. Knobloch, Phys. Rev. Lett. **95**, 244501 (2005).
6. O. Batiste and E. Knobloch, in *Bifurcation Theory and Spatio-Temporal Pattern Formation*, W. Nagata and N. Sri Namachchivaya (eds), Fields Institute Communications **49**, 9 (2006).
7. O. Batiste, I. Mercader, N. Net and E. Knobloch, Phys. Rev. E **59**, 6730 (1999).
8. O. Batiste, E. Knobloch, I. Mercader and M. Net, Phys. Rev. E **65**, 016303 (2001).
9. O. Batiste, E. Knobloch, A. Alonso and I. Mercader, J. Fluid Mech. **560**, 149 (2006).
10. M. Beck, J. Knobloch, D. J. B. Lloyd, B. Sandstede and T. Wagenknecht, SIAM J. Math. Anal. **41**, 936 (2009).
11. A. Bergeon and E. Knobloch, Phys. Fluids **20**, 034102 (2008).
12. A. Bergeon and E. Knobloch, Proc. 3rd Int. Symp. on Bifurcations and Instabilities in Fluid Dynamics, Nottingham, UK (August 2009).
13. A. Bergeon, J. Burke, E. Knobloch and I. Mercader, Phys. Rev. E **78**, 046201 (2008).
14. S. Blanchflower, Phys. Lett. A **261**, 74 (1999).
15. S. Blanchflower and N. O. Weiss, Phys. Lett. A **294**, 297 (2002).
16. C. S. Bretherton and E. A. Spiegel, Phys. Lett. A **96**, 152 (1983).
17. J. Burke and E. Knobloch, Phys. Rev. E **73**, 056211 (2006).
18. J. Burke and E. Knobloch, Phys. Lett. A **360**, 681 (2007).
19. J. Burke and E. Knobloch, Chaos **17**, 037102 (2007).
20. J. Burke and E. Knobloch, Discrete and Continuous Dyn. Syst. Suppl., pp. 109-117 (2009).
21. J. Burke, S. M. Houghton and E. Knobloch, Phys. Rev. E **80**, 036202 (2009).
22. D. R. Caldwell, J. Fluid Mech. **64**, 347 (1974).
23. S. J. Chapman and G. Kozyreff, Physica D **238**, 319 (2009).
24. T. Clune and E. Knobloch, Physica D **61**, 106 (1992).
25. P. Coullet, C. Riera and C. Tresser, Phys. Rev. Lett. **84**, 3069 (2000).
26. G. Dangelmayr and E. Knobloch, Nonlinearity **4**, 399 (1991).
27. J. H. P. Dawes, J. Fluid Mech. **570**, 385 (2007).
28. Q. Feng, J. V. Moloney and A. C. Newell, Phys. Rev. A **50**, R3601 (1994).
29. K. Ghorayeb and A. Mojtabi, Phys. Fluids **9**, 2339 (1997).
30. R. Heinrichs, G. Ahlers and D. S. Cannell, Phys. Rev. A **35**, 2761 (1987).
31. E. Knobloch, Phys. Rev. A **34**, 1538 (1986).
32. E. Knobloch, Nonlinearity **21**, T45 (2008).
33. E. Knobloch and D. R. Moore, Phys. Rev. A **37**, 860 (1988).
34. E. Knobloch, D. R. Moore, J. Toomre and N. O. Weiss, J. Fluid Mech. **166**, 409 (1986).
35. P. Kolodner, Phys. Rev. A **43**, 2827 (1991).

36. P. Kolodner, C. M. Surko and H. Williams, Physica D **37**, 319 (1989).
37. P. Kolodner, J. A. Glazier and H. L. Williams, Phys. Rev. Lett. **65**, 1579 (1990).
38. G. Kozyreff and S. J. Chapman, Phys. Rev. Lett. **97**, 044502 (2006).
39. I. Mercader, A. Alonso and O. Batiste, Eur. Phys. J. E **15**, 311 (2004).
40. I. Mercader, A. Alonso and O. Batiste, Phys. Rev. E **77**, 036313 (2008).
41. I. Mercader, O. Batiste, A. Alonso and E. Knobloch, Phys. Rev. E **80**, 025201(R) (2009).
42. I. Mercader, O. Batiste, A. Alonso and E. Knobloch, Fluid Dyn. Res. **42**, 025505 (2010).
43. I. Mercader, O. Batiste, A. Alonso and E. Knobloch, J. Fluid Mech., submitted.
44. E. Moses, J. Fineberg and V. Steinberg, Phys. Rev. A **35**, 2757 (1987).
45. Y. Pomeau, Physica D **23**, 3 (1986).
46. H. Riecke, Phys. Rev. Lett. **68**, 301 (1992).
47. T. M. Schneider, J. F. Gibson and J. Burke, Phys. Rev. Lett., in press.
48. A. Spina, J. Toomre and E. Knobloch, Phys. Rev. E **57**, 524 (1998).
49. V. Steinberg, J. Fineberg, E. Moses and I. Rehberg, Physica D **37**, 359 (1989).
50. P. D. Woods and A. R. Champneys, Physica D **129**, 147 (1999).
51. H. Yahata, Prog. Theor. Phys. **85**, 933 (1991).